Dalton Transactions

ROYAL SOCIETY OF CHEMISTRY

PAPER

View Article Online
View Journal | View Issue

Cite this: *Dalton Trans.*, 2024, **53**, 15198

Is pentavalent Pr(v) feasible in solid $CsPrF_6$?†

Lian-Wei Ye,[a] Zi-He Zhang,[a] Yang He,[a] Shi-Ru Wei,[a] Jun-Bo Lu,[b] Han-Shi Hu *[a] and Jun Li *[a,b]

Received 17th July 2024,
Accepted 19th August 2024

DOI: 10.1039/d4dt02063d

rsc.li/dalton

The oxidation state (OS) holds significant importance in the field of chemistry and serves as a crucial parameter for tracking electrons. Lanthanide (Ln) elements predominately exhibit a +III oxidation state, with a few elements such as Ce, Pr, Nd, Tb, and Dy able to achieve a +IV oxidation state. Over the past century, numerous attempts to synthesize Pr(v) have been made without success until recent reports on Pr(v) oxides and nitride-oxide in the gas phase expanded our understanding of Ln elements. However, the formation of Pr(v) in the condensed phase remains an open question. In this work, based on advanced quantum chemical investigations, we predict that formation of the solid-state $CsPr^{V}F_6$ from Pr(III) and Pr(IV) complexes is exothermic, indicating that $CsPr^{V}F_6$ is stable. The crystal structure comprises $[PrF_6]^-$ octahedral clusters occupying the interstitial spaces of Cs cations. Electronic structure analysis reveals that the $CsPrF_6$ crystal has a closed-shell structure and that Pr reaches its highest oxidation state of +v. The results indicate that the existence of Pr(v) in solid-state Ln fluorides is not impossible, which enriches our understanding of high-valence Ln compounds.

Introduction

The concept of oxidation state (OS) stands out as one of the fundamental principles in chemistry.[1–4] Exploring the upper limits of an element's OS has long captured the interest of chemists.[5–12] Investigating compounds with high OS deepens our comprehension of chemical elements and paves the way for developing novel oxidants,[13,14] catalysts,[15,16] and other chemical entities.[17,18] In recent decades, the study of Ln chemistry has attracted increased attention, driven by advancements in experimental technologies that facilitate the synthesis of high OS complexes.[6,19,20] Ln compounds are predominantly characterized by the prevalence of the +III OS, primarily due to the inert nature of 4f orbitals resulting from contracted radial distribution and the relatively low energy.[21–23] Only a handful of elements exhibit a high-valent +IV, such as Ce, Pr, Nd, Tb, and Dy.[24–30]

Regarding Ln elements with a higher +v OS, Langmuir predicted as early as 1919 that it could appear in the element Pr, which has the fifth lowest ionization energy.[31] However, the inertness of the 4f orbitals in Ln elements makes achieving a +v OS in compounds a challenging task. The report in 1938 suggested the possibility of Pr(v) formation at 15 bar pressure.[32] However, subsequent research in 1950 conclusively demonstrated that Pr(IV) is the highest OS formed under a higher pressure of 50 bar of oxygen. This was observed when mixtures of Pr_2O_3–Nd_2O_3 and Pr_2O_3–CeO_2 were heated at 300 °C.[33,34] In 2015, efforts using the highly electronegative element fluorine aimed to generate PrF_5 molecules through the laser ablation method. However, conclusive evidence of their formation has not been obtained.[25] Up until 2016, both experimental and theoretical studies have unveiled the existence of Pr(v) in the gas phase, exemplified by oxide species PrO_4 and PrO_2^+, and nitride-oxides NPrO.[19,20] Theoretical research continues to explore potential gas phase Pr(v) molecules,[35,36] while the next objective is to propose an alternative strategy for expanding the Ln OS beyond the gas phase (Scheme 1).

In pursuit of solid-state Pr(v), we confined octahedral $[PrF_6]^-$ clusters within the Cs^+ lattice to achieve $CsPrF_6$ (Scheme 2). A global-minimum search algorithm based on first-principles plane-wave density functional theory (DFT) was employed to elucidate the crystal structure. A comprehensive analysis was conducted, covering stability, electronic structure, chemical bonding, and notably, oxidation state. This discovery provides concrete evidence for the first instance of Pr(v) within a solid state.

Results and discussion

Structure and stability of $CsPrF_6$

To find the stable structure of $CsPrF_6$, the evolutionary algorithm USPEX (Universal Structure Predictor: Evolutionary

[a]*Department of Chemistry and Engineering Research Center of Advanced Rare-Earth Materials of Ministry of Education, Tsinghua University, Beijing 100084, China. E-mail: hshu@mail.tsinghua.edu.cn, junli@tsinghua.edu.cn*

[b]*Fundamental Science Center of Rare Earths, Ganjiang Innovation Academy, Chinese Academy of Sciences, Ganzhou 341000, China*

†Electronic supplementary information (ESI) available: theoretical and computational details. See DOI: https://doi.org/10.1039/d4dt02063d

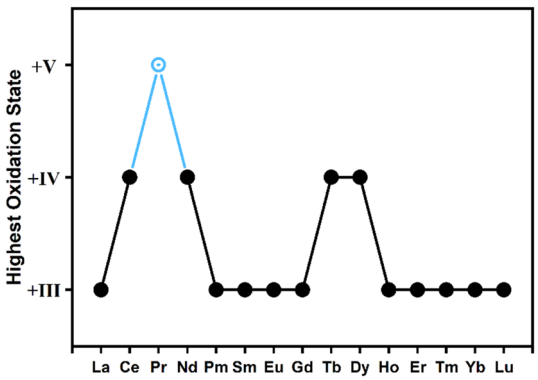

Scheme 1 The highest OS of the 4f-block Ln elements. (●) Highest experimentally known species, (•) the Pr(v) molecule only identified in gas phase.

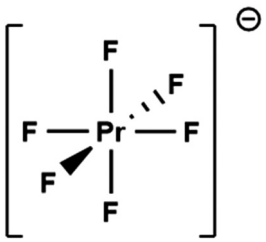

Scheme 2 A schematic structure of the $[PrF_6]^-$ octahedral cluster.

Xtallography) was used, which has been successfully utilized to search for the most thermodynamically stable structures of systems with a fixed composition. The trial structures generated by USPEX were fully relaxed and their final energies evaluated based on first-principles density functional theory (DFT). The density functional computations were carried out using the Vienna *ab initio* simulation package (VASP). A total of 246 trial structures were calculated, and Fig. 1 shows the most stable predicted $CsPrF_6$ structure.

The $CsPrF_6$ structure shown in Fig. 1 belongs to the rhombohedral $R\bar{3}$ phase, which is a $KAsF_6$-type structure and is also

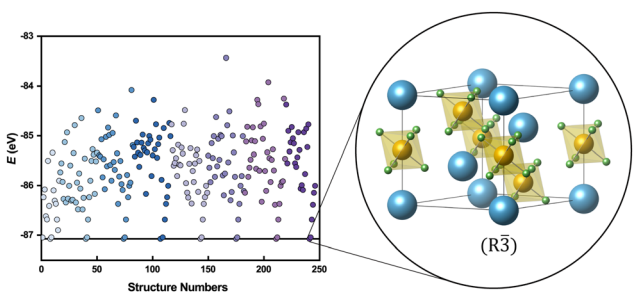

Fig. 1 Prediction of the crystal structure of $CsPrF_6$. Left: the progress of an evolutionary simulation (black line shows the lowest energy as a function of generation, light blue to dark purple circles present different generations). Right: the most stable $R\bar{3}$ $CsPrF_6$ structure (colour scheme: blue: Cs; yellow: Pr; green: F).

observed in KPF_6 and $CsNbF_6$ crystals. Detailed lattice parameters are provided in Table S1,† and the atomic coordinates are given in the ESI, section VI.† The distance between Pr and F atoms is 2.079 Å, representing a moderate bond length compared to the Pr–F distances ranging from 1.994 to 2.109 Å in PrF_n(n = 1–5) molecules.[25] This observation indicates the formation of $[PrF_6]^-$ clusters within the interstitial spaces of Cs cations. The Madelung energy in this arrangement is calculated to be −145.3 eV for the $CsPrF_6$ primitive cell, stabilizing the $[PrF_6]^-$ cluster and enabling the existence of the pentavalent praseodymium anion cluster $[PrF_6]^-$ in the $CsPrF_6$ crystal. This provides a further explanation for the presence of $[PrF_6]^-$. The optimal $CsPrF_6$ structure from global-minimum searching has been further confirmed to be stable in dynamics using phonon spectrum calculations along the high-symmetry lines in the Brillouin zone, as shown in Fig. S2.† There are no obvious imaginary vibrational frequencies in the phonon spectrum, suggesting the dynamic stability of the structure.

To demonstrate the thermodynamic stability of the $CsPrF_6$ crystal, a possible synthetic pathway is depicted in Table 1, eqn (1) and (2). The Gibbs free energy of formation ($\Delta G_{300\ K}$) at a temperature of 300 K was calculated using the formula $\Delta G_{300\ K} = G(CsPrF_6) - G(PrF_3) - G(F_2)$ or $\Delta G_{300\ K} = G(CsPrF_6) + G(CsF) - G(Cs_2PrF_6) - 1/2\ G(F_2)$, respectively. Here, G represents the energy with entropy and zero-point energy correction for different species. Importantly, all calculated $\Delta G_{300\ K}$ values are negative, signifying that the formation of the $CsPrF_6$ solid is energetically favourable under these conditions. Notably, the reactants F_2, CsF[37] and PrF_3[38] mentioned in eqn (1) are naturally occurring, with PrF_3 being a common raw material for synthesizing Pr fluorides in the laboratory,[39] which outlines plausible methods for synthesizing $CsPrF_6$. Comprehensive thermodynamic free energy data for the reactants in the equations can be found in Table S2.†

To further examine the thermal stability of the predicted $CsPrF_6$, a series of AIMD simulations was carried out at various temperatures of 300 K, 600 K, 900 K and 1200 K for a duration of 10 ps, respectively. Since the distances between Pr and other atoms reflect the structural integrity, the radial distribution function (RDF) of the neighbouring Pr–F and Pr–Cs distances is a good parameter for quantitatively evaluating the structural deformation of $CsPrF_6$. The RDFs of AIMD simulations at different temperatures are shown in Fig. 2, with a sharp Pr–F peak around 2.1 Å and clear Pr–Cs peak around 4.0 and 4.6 Å at 300 K after 10 ps simulations, indicating stability at room temperature. As expected, at a relatively high temperature of 600 K, the peaks show a little more dispersion, and much more disorder appears at 900 K. Once the temperature

Table 1 Plausible methods for synthesizing $CsPrF_6$ and its reaction free energy (kcal mol^{-1})

Reaction	$\Delta G_{300\ K}$	
$PrF_3(s) + F_2(g) + CsF(s) \rightarrow CsPrF_6(s)$	−74.1	(1)
$Cs_2PrF_6(s) + \frac{1}{2}F_2(g) \rightarrow CsPrF_6(s) + CsF(s)$	−133.2	(2)

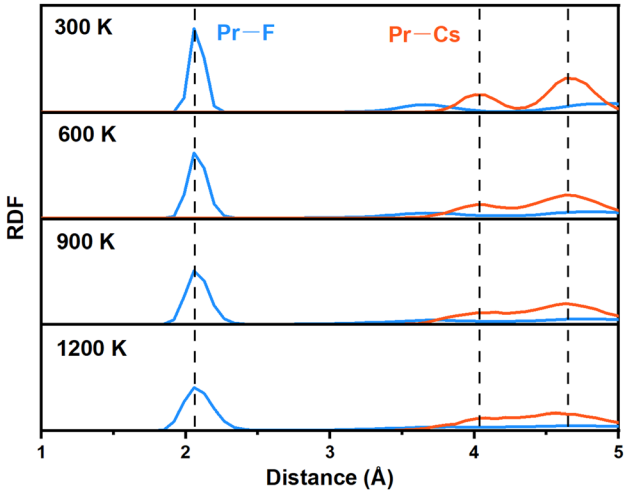

Fig. 2 The radial distribution function (RDF) of Pr and other atoms such as F and Cs respectively at different temperatures for spin-polarized calculations.

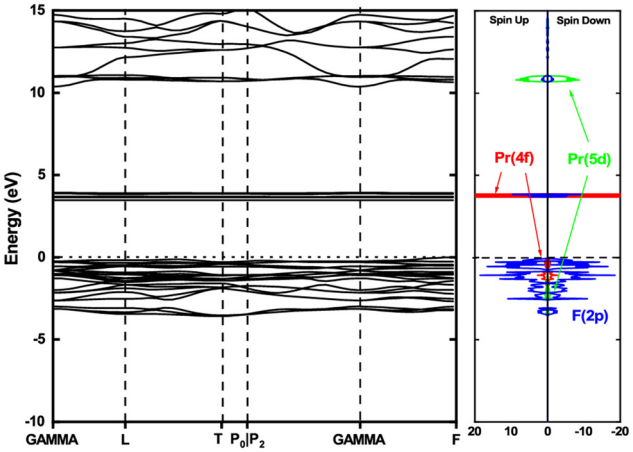

Fig. 3 The HSE06 band and partial density of states (pDOS) of the $CsPr^{V}F_6$ crystal. The Fermi level is assigned at 0 eV.

reaches 1200 K, the Pr–Cs peak becomes indistinguishable and the Pr–F peak disperses even further, indicating that the structure is not stable at this high temperature.

Chemical bonding and oxidation state analysis

The stability of the $CsPrF_6$ crystal relies on its electronic structure. A detailed examination of the electronic structure was conducted, using the band structure, density of states (DOS), spin density, crystal orbital Hamiltonian population (COHP), and Bader charge analysis. Furthermore, the electronic structural properties of $CsPrF_6$ were compared with those of Pr-containing complexes featuring different OS, specifically $CsPr^{II}F_3$,[40] $Cs_3P^{III}rF_6$,[41] and $Cs_2Pr^{IV}F_6$.[41] In the subsequent analyses, we conducted a comprehensive comparison of the properties of Pr across formal OS +II to +V compounds, delving into electron occupancy, orbital interactions, and chemical bonding in various Pr complexes

The band structure and related properties of $CsPrF_6$ are presented in Fig. 3. A sizable band gap appears in the $CsPrF_6$ crystal between the filled and empty states, of approximately 3.5 eV at the HSE06 hybrid functional level, indicating that it is a potential semiconductor material. The band structures of different Pr-containing complexes were calculated along the high-symmetry directions in the Brillouin zone (BZ) as illustrated in Fig. S11–13.†

The interactions between different orbitals can be illustrated through the DOS analysis shown in Fig. 3. The inner 4f orbitals are a distinctive characteristic of Ln elements, deemed "core-like" due to their minimal participation in chemical bonding, as evident from the sharp distribution in DOS. Until Pr reaches its highest OS, unpaired electrons occupy the 4f orbitals below the Fermi level (Fig. S14–16†). However, in the $CsPrF_6$ compound, the majority of Pr 4f orbitals extend beyond the Fermi level (approximately 4 eV), indicating significant hybridization with the F 2p orbitals (Fig. 3). This implies that the 4f orbitals of Pr are unfilled, contributing to Pr attaining its highest +V OS. The results are attributed to the higher energy of Pr 4f orbitals compared to F 2p in $CsPrF_6$, facilitating electron transfer from Pr to F. The Pr 5d orbitals exhibit a greater dispersion than 4f orbitals, allowing for enhanced interaction with the F element. In the $CsPrF_6$ compound, the bonding and antibonding orbitals of 5d show significant separation. The 5d antibonding orbitals of Pr are located approximately 11 eV above the Fermi level, while the bonding orbitals are distributed in the energy range of −4 to −1 eV. This dispersed band indicates a non-negligible interaction with F 2p (Fig. 3). Similar trends are observed in other Pr compounds (Fig. S14–16†), indicating a prevalent utilization of Pr 5d orbitals for bonding. Further quantitative analysis of the COHP to emphasize the importance of the 5d orbitals in the bonding mechanism of $CsPrF_6$ can be found in the next section.

Due to the inherently inner and unpaired nature of 4f electrons, the analysis of spin density serves as another powerful tool to illustrate their localization. The spin densities of different Pr-containing compounds are depicted in Fig. S17–20.† Unpaired electrons are not observed in $CsPr^{V}F_6$, whereas they are prominently displayed in $CsPr^{II}F_3$, $Cs_3P^{III}rF_6$, and $Cs_2Pr^{IV}F_6$. This suggests that the inner 4f electrons of Pr in $CsPrF_6$ have been removed, indicating a +V OS.

To elucidate the bonding mechanism in the $CsPrF_6$ crystal, COHP analysis was applied to evaluate the population of wavefunctions on the atomic orbitals' overlap of selected atom pairs. The integrated COHP (ICOHP) for the bonded Pr–F in $CsPrF_6$ is −5.94 eV per pair up to the Fermi level, indicating some covalent interaction between the Pr and F atoms, as shown in Fig. 4. Specifically, the covalent interaction between Pr 5d and F 2p is stronger than that of Pr 4f, where the 4f orbitals of Pr play an insignificant role in chemical bonding due to their inner nature. The COHP analysis for other compounds with different OS of Pr is provided in Fig. S21–23.† For example, the ICOHP value for the Pr–F bond is −2.58 eV for

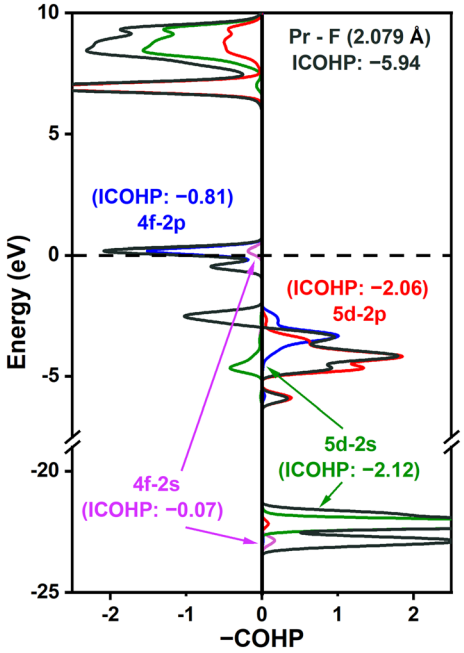

Fig. 4 The crystal orbital Hamilton population (COHP) analysis of Pr–F interactions in solid-state $CsPrF_6$. Zero line (dotted) represents the Fermi level. The ICOHP values (in eV per bond) are listed here to show the corresponding interactions (black) and main orbital-pair contributions to these (coloured). There are six Pr–F bonds in a $CsPrF_6$ cell.

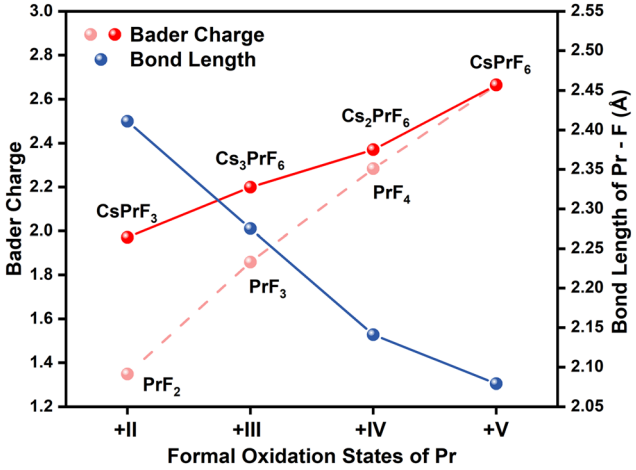

Fig. 5 The calculated Pr Bader charge and Pr–F bond lengths in $CsPr^{II}F_3$, $Cs_3Pr^{III}F_6$, $Cs_2Pr^{IV}F_6$, $CsPr^{V}F_6$ crystals and PrF_n (n = 2–4) compounds.

$CsPrF_3$, −2.09 eV for Cs_3PrF_6, and −5.04 eV for Cs_2PrF_6. The $CsPrF_6$ crystal exhibits a moderate ICOHP value among them.

Usually, the formal OS of a central atom in a coordination sphere is defined as the charge of the central atom when every ligand of the coordination sphere is removed in its most stable form. The bonding electron pairs between the metal center and the ligand are therefore exclusively assigned to the more electronegative fragment, resulting in a negative OS.[6] Therefore, the OS of fluorine and cesium are considered as −I and +I, respectively. According to these rules, the oxidation number of praseodymium in the $CsPrF_6$ solid is +V. To further support this, we calculated the charges using Bader's quantum theory of atoms in molecules (QTAIM) for the $CsPrF_6$ solid.[42–44] In QTAIM analysis, the charges of an atom are calculated by integrating the charge density in the surrounding basin, partitioned by the stationary points of the charge density.

In Fig. 5, various Pr-containing complexes are presented. The Bader charges for the central Pr atom are 1.97, 2.20, 2.37, and 2.66 for $CsPr^{II}F_3$, $Cs_3Pr^{III}F_6$, $Cs_2Pr^{IV}F_6$, and $CsPr^{V}F_6$, respectively. The $CsPrF_6$ solid exhibits the highest Bader charge, which is consistent with the formal OS of Pr in the $CsPrF_6$ solid which is +V as mentioned above. It is common for the Bader charge to increase as the OS increases in similar compounds. This trend is evident in Bader charges of 1.35, 1.86, 2.28, and 2.66 for the standard compounds, $Pr^{II}F_2$, $Pr^{III}F_3$, $Pr^{IV}F_4$, and $CsPr^{V}F_6$, respectively. Additionally, the bond lengths between Pr and F are reported to be 2.411, 2.275, 2.141, and 2.097 Å for the respective complexes. It is observed that as the OS increases, the bond length decreases, and the charge on the praseodymium atom becomes more positive. These findings further confirm that $CsPrF_6$ exists with the Pr (V) formal OS.

Conclusions

In summary, an unexpected solid-state $CsPrF_6$ with Pr(V) was designed and predicted using a global-minimum search method. The crystal structure features a hexahedral $[Pr^{V}F_6]^-$ anion cluster embedded within the Cs^+ lattice. Cs^+ contributes to the Madelung energy, enhancing the stability of the Pr(V) cluster. Gibbs free energy calculations confirm the thermodynamic stability of the crystal, suggesting its potential for experimental synthesis. Phonon calculations provide evidence of its dynamic stability, while AIMD simulations conducted at different temperatures indicate that the crystal remains stable up to 900 K. As anticipated, Bader charge analysis indicates that Pr in $CsPrF_6$ exhibits a +V OS, confirmed by comparing it with different OS of Pr-containing crystals. This finding is further supported by its closed shell electronic structure, where nearly all of the 4f bands are situated above the Fermi level, and no spin density is located at the Pr atom. The prediction of the $CsPrF_6$ crystal suggests that the highest known OS of Ln(V) is achievable in the solid state and proposes a stabilizing strategy for obtaining high-valent fluorides.

Computational details

The structure of complexes CsF (mp-1784),[37] PrF_3 (ICSD-77741),[38] $CsPrF_3$ (OQMD-1706464),[40] Cs_3PrF_6 (mp-1206084),[41] and Cs_2PrF_6 (OQMD-1282041)[41] were obtained from different databases. The lowest-enthalpy $CsPrF_6$ structure was searched using the evolutionary algorithm USPEX 9.4.4.[45–48] The calculations were carried out for the best structure that no

longer changed for 8 generations and each generation of structures was obtained by applying heredity (50%), softmutation (20%), and lattice mutation (10%) operators, while some were produced randomly from the space group (20%).

The geometry of these structures was further optimized based on first-principles density functional theory (DFT) electronic-structure calculations involving the projector-augmented wave (PAW) method[49] as implemented in the Vienna *ab initio* simulation package (VASP)[50] version 5.4.4. The Perdew–Burke–Ernzerhof (PBE) functional[51] was utilized for both structural search and structural relaxation. The energy cutoff for the plane-wave basis was set to 450 eV. The Brillouin zone was sampled using uniform Γ-centered meshes with a resolution of $2\pi \times 0.04$ Å^{-1}. Electronic degrees of freedom were considered converged when the total energy change between two steps was smaller than 10^{-7} eV. All atoms were fully relaxed until the Hellmann–Feynman forces fell below 0.01 eV Å^{-1}. The Madelung energy of the optimized $CsPrF_6$ primitive structure was calculated using VESTA software.[52] To explore the thermal stability, *ab initio* molecular (AIMD) simulations were carried out using VASP with the canonical (NVT) ensemble and a Nosé–Hoover thermostat.[53,54] The simulations lasted for 10 ps at temperatures of 300, 600, 900, and 1200 K, with a time step of 1 fs. To assess the dynamic stability, the finite displacement method was used for phonon dispersion calculations within the Phonopy program.[55] For the chemical bonding analysis, we utilized the COHP method[56,57] as calculated using the LOBSTER package.[58,59] During the orbital projection, the basis sets pbeVasp2015[59] were used with additional functions fitted to atomic VASP GGA-PBE wave functions. For charge population analysis, Bader's quantum theory of atoms in molecules (QTAIM) was used for the solids.[42–44]

In order to account for the correlation effects involving 4f electrons and obtain a more accurate electronic structure, the Heyd–Scuseria–Ernzerhof (HSE06) hybrid functional was applied to obtain more accurate band structures and density of states (DOS). The Brillouin zone was sampled using uniform Γ-centered meshes with a resolution of $2\pi \times 0.04$ Å^{-1}. For the band structure calculations, 78, 65, 50, and 56 *k*-points were used for the $CsPrF_3$, Cs_3PrF_6, Cs_2PrF_6, and $CsPrF_6$ crystal structures, respectively. The self-consistent field convergence criterion was set to 10^{-5} eV.[60]

Author contributions

J. L. designed the project. L. W. Y. performed the computational calculations. L. W. Y., Z. H. Z., Y. H., S. R. W., J. B. L., H. S. H. and J. L. wrote and edited the manuscript. All authors helped to analyse the theoretical results.

Data availability

The data supporting this article have been included in the ESI.† All data from DFT calculations involved in this work can be found in the article and ESI.†

Conflicts of interest

There are no conflicts to declare.

Acknowledgements

This work was supported by the National Key Research and Development Project (No. 2022YFA1503900, 2022YFA1503000), the National Natural Science Foundation of China (NSFC No. 22033005, 22222605 and 22076095), and the Guangdong Provincial Key Laboratory of Catalysis (No. 2020B121201002). The calculations were performed using supercomputers at the High Performance Computing Center of Tsinghua University. The Tsinghua Xuetang Talents Program is acknowledged for providing computational resources.

References

1 L. J. Malone and T. Dolter, *Basic concepts of chemistry*, John Wiley & Sons, 2008.
2 F. A. Cotton, G. Wilkinson, C. A. Murillo and M. Bochmann, *Advanced inorganic chemistry*, John Wiley and Sons, Inc., 1999.
3 N. N. Greenwood and A. Earnshaw, *Chemistry of the Elements*, Elsevier, 2012.
4 P. Karen, P. McArdle and J. Takats, Comprehensive definition of oxidation state (IUPAC Recommendations 2016), *Pure Appl. Chem.*, 2016, **88**, 831–839.
5 S. N. Achary and A. K. Tyagi, in *Handbook on Synthesis Strategies for Advanced Materials: Volume-III: Materials Specific Synthesis Strategies*, ed. A. K. Tyagi and R. S. Ningthoujam, Springer Singapore, Singapore, 2021, pp. 137–158.
6 G. Wang, M. Zhou, J. T. Goettel, G. J. Schrobilgen, J. Su, J. Li, T. Schlöder and S. Riedel, Identification of an iridium-containing compound with a formal oxidation state of IX, *Nature*, 2014, **514**, 475–477.
7 P. Pyykkö and W.-H. Xu, The formal oxidation states of iridium now run from −III to +IX, *Angew. Chem., Int. Ed.*, 2015, **54**, 1080–1081.
8 Z.-L. Xue, $[IrO_4]$+ at the IX (+9) oxidation state observed, report states, *Sci. China: Chem.*, 2015, **58**, 4–5.
9 P. Pyykkö and W.-H. Xu, On the extreme oxidation states of iridium, *Chem. – Eur. J.*, 2015, **21**, 9468–9473.
10 S.-X. Hu, W.-L. Li, J.-B. Lu, J. L. Bao, H. S. Yu, D. G. Truhlar, J. K. Gibson, J. Marçalo, M. Zhou, S. Riedel, W. H. E. Schwarz and J. Li, On the upper limits of oxidation states in chemistry, *Angew. Chem., Int. Ed.*, 2018, **57**, 3242–3245.
11 P. Pyykkö, N. Runeberg, M. Straka and K. G. Dyall, Could uranium(XII)hexoxide, UO_6 (Oh) exist?, *Chem. Phys. Lett.*, 2000, **328**, 415–419.
12 H. Xiao, H.-S. Hu, W. H. E. Schwarz and J. Li, Theoretical investigations of geometry, electronic structure and stabi-

lity of UO_6: Octahedral uranium hexoxide and its isomers, *J. Phys. Chem. A*, 2010, **114**, 8837–8844.
13 J. H. Canterford and T. A. O'Donnell, Reactivity of transition metal fluorides. IV. Oxidation-reduction reactions of vanadium pentafluoride, *Inorg. Chem.*, 1967, **6**, 541–544.
14 B. C. Bales, P. Brown, A. Dehestani and J. M. Mayer, Alkane oxidation by osmium tetroxide, *J. Am. Chem. Soc.*, 2005, **127**, 2832–2833.
15 N. Bartlett, The oxidizing properties of the third transition series hexafluorides and related compounds, *Angew. Chem., Int. Ed. Engl.*, 1968, **7**, 433–439.
16 B. L. Pagenkopf and E. M. Carreira, Transition metal fluoride complexes in asymmetric catalysis, *Chem. – Eur. J.*, 1999, **5**, 3437–3442.
17 W. W. Dukat, J. H. Holloway, E. G. Hope, M. R. Rieland, P. J. Townson and R. L. Powell, High oxidation state binary transition metal fluorides as selective fluorinating agents, *J. Chem. Soc., Chem. Commun.*, 1993, **1993**, 1429–1430.
18 J. H. Holloway, E. G. Hope, P. J. Townson and R. L. Powell, Selective fluorination of dichloromethane by highest oxidation state transition-metal oxide fluorides, *J. Fluor. Chem.*, 1996, **76**, 105–107.
19 Q. Zhang, S.-X. Hu, H. Qu, J. Su, G. Wang, J.-B. Lu, M. Chen, M. Zhou and J. Li, Pentavalent lanthanide compounds: formation and characterization of praseodymium (v) oxides, *Angew. Chem., Int. Ed.*, 2016, **55**, 6896–6900.
20 S.-X. Hu, J. Jian, J. Su, X. Wu, J. Li and M. Zhou, Pentavalent lanthanide nitride-oxides: NPrO and $NPrO^-$ complexes with NPr triple bonds, *Chem. Sci.*, 2017, **8**, 4035–4043.
21 P. B. Hitchcock, M. F. Lappert, L. Maron and A. V. Protchenko, Lanthanum does form stable molecular compounds in the +2 oxidation state, *Angew. Chem., Int. Ed.*, 2008, **47**, 1488–1491.
22 M. R. MacDonald, J. E. Bates, J. W. Ziller, F. Furche and W. J. Evans, Completing the series of +2 ions for the lanthanide elements: Synthesis of molecular complexes of Pr^{2+}, Gd^{2+}, Tb^{2+}, and Lu^{2+}, *J. Am. Chem. Soc.*, 2013, **135**, 9857–9868.
23 W.-L. Li, C. Ertural, D. Bogdanovski, J. Li and R. Dronskowski, Chemical bonding of crystalline LnB_6 (Ln = La–Lu) and its relationship with Ln_2B_8 gas-phase complexes, *Inorg. Chem.*, 2018, **57**, 12999–13008.
24 A. Schulz and J. F. Liebman, Paradoxes and paradigms: High oxidation states and neighboring rows in the periodic table—Lanthanides, actinides, exotica and explosives, *Struct. Chem.*, 2008, **19**, 633–635.
25 T. Vent-Schmidt and S. Riedel, Investigation of praseodymium fluorides: A combined matrix-isolation and quantum-chemical study, *Inorg. Chem.*, 2015, **54**, 11114–11120.
26 A. F. Lucena, C. Lourenço, M. C. Michelini, P. X. Rutkowski, J. M. Carretas, N. Zorz, L. Berthon, A. Dias, M. Conceição Oliveira, J. K. Gibson and J. Marçalo, Synthesis and hydrolysis of gas-phase lanthanide and actinide oxide nitrate complexes: A correspondence to trivalent metal ion redox potentials and ionization energies, *Phys. Chem. Chem. Phys.*, 2015, **17**, 9942–9950.
27 S. Gabelnick, G. Reedy and M. Chasanov, Infrared spectra and structure of some matrix–isolated lanthanide and actinide oxides, *J. Chem. Phys.*, 1974, **60**, 1167–1171.
28 Z. Mazej, Room temperature syntheses of lanthanoid tetrafluorides (LnF_4, Ln= Ce, Pr, Tb), *J. Fluor. Chem.*, 2002, **118**, 127–129.
29 V. I. Spitsyn, Y. M. Kiselev, L. I. Martynenko, V. N. Prusakov and V. B. Sokolov, Synthesis of praseodymium tetrafluoride, *Dokl. Akad. Nauk SSSR (USSR)*, 1974, **219**, 621–624.
30 T. Vent-Schmidt, Z. Fang, Z. Lee, D. Dixon and S. Riedel, Extending the row of lanthanide tetrafluorides: A combined matrix-isolation and quantum-chemical study, *Chem. – Eur. J.*, 2016, **22**, 2406–2416.
31 I. Langmuir, The arrangement of electrons in atoms and molecules, *J. Am. Chem. Soc.*, 1919, **41**, 868–934.
32 W. Prandtl and G. Rieder, Über die Wertigkeit des Praseodyms und des Terbiums, *Z. Anorg. Allg. Chem.*, 1938, **238**, 225–235.
33 J. D. McCullough, An X-ray study of the rare-earth oxide systems: Ce^{IV}—Nd^{III}, Cr^{IV}—Pr^{III}, Ce^{IV}—Pr^{IV} and Pr^{IV}—Nd^{III}, *J. Am. Chem. Soc.*, 1950, **72**, 1386–1390.
34 J. Kleinberg, Unfamiliar oxidation states: Recent progress, *J. Chem. Educ.*, 1952, **29**, 324.
35 W.-J. Zhang, G.-J. Wang, P. Zhang, W. Zou and S.-X. Hu, The decisive role of 4f-covalency in the structural direction and oxidation state of XPrO compounds (X: group 13 to 17 elements), *Phys. Chem. Chem. Phys.*, 2020, **22**, 27746–27756.
36 P. S. Piotr, G. Szkudlarek and W. Grochala, Limits of stability for compounds of pentavalent praseodymium, *arXiv*, 2023, DOI: **10.48550/arXiv.2306.13939**.
37 E. Posnjak and R. W. G. Wyckoff, The crystal structures of the alkali halides. II, *J. Wash. Acad. Sci.*, 1922, **12**, 248–251.
38 O. Greis, R. Ziel, B. Breidenstein, A. Haase and T. Petzel, Structural data of the tysonite-type superstructure modification β-PrF_3 from X-ray powder and electron single-crystal diffraction, *Powder Diffr.*, 1995, **10**, 44–46.
39 R. Hoppe and W. Liebe, Komplexe Fluoride des vierwertigen Praseodyms, *Z. Anorg. Allg. Chem.*, 1961, **313**, 221–227.
40 J. E. Saal, S. Kirklin, M. Aykol, B. Meredig and C. Wolverton, Materials design and discovery with high-throughput density functional theory: The Open Quantum Materials Database (OQMD), *JOM*, 2013, **65**, 1501–1509.
41 A. Jain, S. P. Ong, G. Hautier, W. Chen, W. D. Richards, S. Dacek, S. Cholia, D. Gunter, D. Skinner, G. Ceder and K. A. Persson, Commentary: The Materials Project: A materials genome approach to accelerating materials innovation, *APL Mater.*, 2013, **1**, 011002.
42 G. Henkelman, A. Arnaldsson and H. Jónsson, A fast and robust algorithm for Bader decomposition of charge density, *Comput. Mater. Sci.*, 2006, **36**, 354–360.
43 E. Sanville, S. D. Kenny, R. Smith and G. Henkelman, Improved grid-based algorithm for Bader charge allocation, *J. Comput. Chem.*, 2007, **28**, 899–908.
44 W. Tang, E. Sanville and G. Henkelman, A grid-based Bader analysis algorithm without lattice bias, *J. Phys.: Condens. Matter*, 2009, **21**, 084204.

45 A. R. Oganov and C. W. Glass, Crystal structure prediction using ab initio evolutionary techniques: Principles and applications, *J. Chem. Phys.*, 2006, **124**, 244704.
46 A. O. Lyakhov, A. R. Oganov, H. T. Stokes and Q. Zhu, New developments in evolutionary structure prediction algorithm USPEX, *Comput. Phys. Commun.*, 2013, **184**, 1172–1182.
47 A. R. Oganov, A. O. Lyakhov and M. Valle, How evolutionary crystal structure prediction works—And why, *Acc. Chem. Res.*, 2011, **44**, 227–237.
48 A. R. Oganov, Y. Ma, A. O. Lyakhov, M. Valle and C. Gatti, Evolutionary crystal structure prediction as a method for the discovery of minerals and materials, *Rev. Mineral. Geochem.*, 2010, **71**, 271–298.
49 P. E. Blöchl, Projector augmented-wave method, *Phys. Rev. B: Condens. Matter Mater. Phys.*, 1994, **50**, 17953–17979.
50 G. Kresse and J. Furthmüller, Efficient iterative schemes for ab initio total-energy calculations using a plane-wave basis set, *Phys. Rev. B: Condens. Matter Mater. Phys.*, 1996, **54**, 11169–11186.
51 J. P. Perdew, K. Burke and M. Ernzerhof, Generalized gradient approximation made simple, *Phys. Rev. Lett.*, 1996, **77**, 3865–3868.
52 K. Momma and F. Izumi, VESTA 3 for three-dimensional visualization of crystal, volumetric and morphology data, *J. Appl. Crystallogr.*, 2011, **44**, 1272–1276.
53 S. Nosé, A unified formulation of the constant temperature molecular dynamics methods, *J. Chem. Phys.*, 1984, **81**, 511–519.
54 W. G. Hoover, Canonical dynamics: Equilibrium phase-space distributions, *Phys. Rev. A*, 1985, **31**, 1695–1697.
55 A. Togo and I. Tanaka, First principles phonon calculations in materials science, *Scr. Mater.*, 2015, **108**, 1–5.
56 R. Dronskowski and P. E. Bloechl, Crystal orbital Hamilton populations (COHP): Energy-resolved visualization of chemical bonding in solids based on density-functional calculations, *J. Chem. Phys.*, 1993, **97**, 8617–8624.
57 V. L. Deringer, A. L. Tchougréeff and R. Dronskowski, Crystal orbital Hamilton population (COHP) analysis as projected from plane-wave basis sets, *J. Phys. Chem. A*, 2011, **115**, 5461–5466.
58 S. Maintz, V. L. Deringer, A. L. Tchougréeff and R. Dronskowski, Analytic projection from plane-wave and PAW wavefunctions and application to chemical-bonding analysis in solids, *J. Comput. Chem.*, 2013, **34**, 2557–2567.
59 S. Maintz, V. L. Deringer, A. L. Tchougréeff and R. Dronskowski, LOBSTER: A tool to extract chemical bonding from plane-wave based DFT, *J. Comput. Chem.*, 2016, **37**, 1030–1035.
60 J. Heyd, G. E. Scuseria and M. Ernzerhof, Hybrid functionals based on a screened Coulomb potential, *J. Chem. Phys.*, 2003, **118**, 8207–8215.